Following the Shadow: Agile 3-D Beam-Steering for 60 GHz Wireless Networks

Anfu Zhou*, Leilei Wu*, Shaoqing Xu*, Huadong Ma*, Teng Wei†, Xinyu Zhang‡
* Beijing Key Lab of Intell. Telecomm. Software and Multimedia, Beijing University of Posts and Telecomm.
† Department of Electrical and Computer Engineering, University of Wisconsin-Madison
‡ Department of Electrical and Computer Engineering, University of California San Diego
Email: {zhouanfu,layla,donggua,mhd}@bupt.edu.cn, twei7@wisc.edu, xyzhang@ucsd.edu

***Abstract*—60 GHz networks, with multi-Gbps bitrate, are considered as the enabling technology for emerging applications such as wireless Virtual Reality (VR) and 4K/8K real-time Miracast. However, user motion, and even orientation change, can cause mis-alignment between 60 GHz transceivers' directional beams, thus causing severe link outage. Within the practical 3D spaces, the combination of location and orientation dynamics leads to exponential growth of beam searching complexity, which substantially exacerbates the outage and hinders fast recovery. In this paper, we first conduct an extensive measurement to analyze the impact of 3D motion on 60 GHz link performance, in the context of VR and Miracast applications. We find that 3D motion exhibits inherent non-predictability, so conventional beam steering solutions, which targets 2D scenarios with lower search space and short-term motion coherence, fail in practical 3D setup. Motivated by these observations, we propose a model-driven 3D beam-steering mechanism called Orthogonal Scanner (OScan), which can maintain high performance for mobile 60 GHz links in 3D space. OScan discovers and leverages a hidden interaction between 3D beams and the spatial channel profile of 60 GHz radios, and strategically scans the 3D space so as to reduce the search latency by more than one order of magnitude. Experiment results based on a custom-built 60 GHz platform along with a trace-driven emulator demonstrate OScan's remarkable throughput gain, up to 5×, compared with the state-of-the-art.**

I. Introduction

60 GHz technology represents a new paradigm that can boost wireless systems to wire-speed. The recently-ratified 60 GHz MAC/PHY standard, IEEE 802.11ad [1], supports up to 6.7 Gbps, and the coming IEEE 802.11ay [2] will deliver 20 Gbps rate. It is believed that 60 GHz radios will bring wireless access into the multi-Gbps era, for both the out-door cellular picocell [3], [4] and indoor WiFi networks [1]. Moreover, 60 GHz radios will spur ultra-high speed wireless applications such as wireless virtual reality (VR) [5], [6] and 4K real-time Miracast streaming [7].

However, despite the huge potential, some key bottleneck technologies still hinder wide adoption of 60 GHz, the first and foremost being efficient beam-steering. In particular, 60 GHz radios use highly directional beams, in contrast to the conventional omni-directional WiFi/cellular signals below 6 GHz. 60 GHz radios usually pack dozens or even hundreds of antenna elements into a phased-array antenna, which concentrates the signals to form ultra-narrow "pencil beams", thus compensating for the attenuation loss [8]. In consequence, a pair of 60 GHz transceivers can establish a link only after their beams are properly aligned. However, the alignment may become broken due to transceiver movement or obstacle blockage. To realign the beams and recover from link outage, an efficient beam-steering mechanism is highly desired.

Much effort has been devoted to design agile beam-steering, from the hierarchical beam scanning defined in standards [1], [9], to heuristic-based shortcuts [10], [11] or sensing-inspired solutions [12], [13]. However, these methods mainly focus on two dimensional (2D) beam-steering, *e.g.*, assuming a phased-array that can steer the main beam among different angles within a 2D plane. In practice, the users and radios move in 3D space; and a 60 GHz array can comprise a planar "matrix" of antenna elements, steering the beams towards different angles in the 3D space. Under such cases, we find that the *beam steering becomes a far more challenging problem that cannot be addressed by straightforward extension of 2D counterparts*. In particular, *3D movement involves not only location translation, but also orientation changes* (*e.g.*, VR players quickly move, jump and crouch in 3D space), which are fundamentally different from the linear/circular device movement commonly assumed in 2D beam steering solutions. Moreover, the main-lobe and side-lobes inside 3D beams exhibits a more intriguing spatial relation than 2D beams (Sec. III). Due to the compound effect, legacy 2D beam steering solutions can lead to even worse performance than brute-force search, which already entails formidable overhead considering the exponentially-increased search space due to dimension increase (Sec. IV).

In this paper, we conduct a systematic study on 3D beam steering. *First*, we begin with a comprehensive measurement of 3D movement in practical 60 GHz applications, and analyze the corresponding impacts on 60 GHz link dynamics. Using Google Tango [14], we collect accurate and fine-grained motion time-series, including location and orientation, when users are running two typical 60 GHz applications: wireless VR and Miracast. We then examine the 60 GHz link performance by feeding the traces into a custom-built software radio testbed. We find that 3D rotation, in contrast to the translation movement commonly assumed in previous studies, has a much greater impact on channel dynamics and can lead to abrupt link performance degradation in a very short-time scale (*i.e.*, less than 100ms). More importantly, 3D movement under practical applications exhibits an inherent "non-predictability" property, *i.e.*, the mobility pattern, especially the rotation pattern, is hard to predict given the history information. Such non-predictability renders the failure of heuristic based beam-steering shortcuts, which rely on accurate movement prediction.

Second, motivated by the measurement insights, we propose a novel 3D beam-steering mechanism called Orthogonal Scanner (OScan), which reduces steering latency by more than one order of magnitude, in comparison to conventional approaches that ignore the unique issues in 3D space. Note that beam steering is frequently invoked during device movement and the

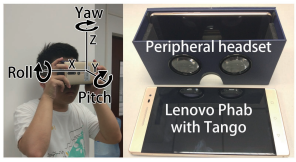

Fig. 1. Mobile VR setup.

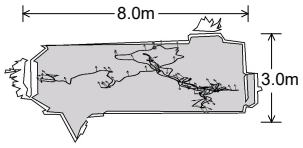

Fig. 2. VR playground.

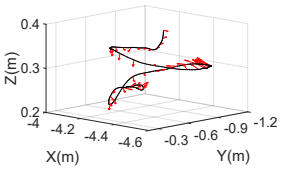

Fig. 3. A segment of VR movement.

Mode	Roll	Pitch	Yaw
Plain	1.07	0.82	2.78
VR	1.49	1.12	7.40
Miracast	3.12	1.66	10.88

TABLE I
AVE. ROTATION(DEG./0.1S)

overhead can even dominate data transmission time. By saving such overhead, OScan can maintain high performance for 60 GHz links under mobility.

OScan is designed based on our discovery that the distribution of channel quality over all 3D beams manifests a "deformed-cross" pattern. Intuitively, the channel response of other beams is like "shadow" of the optimal beam that aligns perfectly with the underlying spatial channel profile (SCP). It is noteworthy that such a unique pattern is *not* tied to any particular beamforming code-book, but roots from the interaction of SCP and any 3D beam designed following general codebook design principles (*e.g.*, consistent with codebook in practical planar phased-arrays). We quantitatively characterize the interaction using a mathematic model. By exploiting the interaction feature, OScan strategically scans the 3D space in a "cross" way (*i.e.*, following the clue of the shadow), in contrast with the conventional time-consuming "blind" trail-and-error approach. Moreover, we also extend the basic cross searching to multi-rounds, each with a deliberate starting beam. In this way, OScan can avoid being trapped in any local-maximum beam and keep its efficiency, even in complicated environment with heterogeneous reflectors.

We implement OScan on a custom-built 60 GHz platform, along with a trace-driven simulator. We evaluate OScan's performance against the default scanning in IEEE 802.11ad [1] and heuristic approach commonly used in state-of-the-art [8], [11]. Experimental results demonstrate that OScan converges quickly to the optimal beam with maximum channel quality, at the cost of less than 20% of the 802.11ad overhead. Overall, the beam optimality and saved scanning time translate into significant throughput gain, up to 5× for the dynamic Miracast. The remarkable gain also reflects how 3D movement can severely undermine nominal Gbps bit-rates of 60 GHz radios, and cause huge channel underutilization under existing 60 GHz protocols.

To our knowledge, OScan represents the first work to investigate how practical 3D movement impacts 60 GHz performance, and to design an agile 3D beam steering mechanism. Our contribution breaks down into the following three aspects:

(i) We perform extensive measurements to examine 3D movement of VR and Miracast. We characterize the unique features of 3D movement and their impact on 60 GHz link dynamics (Sec. II).

(ii) We design an agile 3D beam steering mechanism called OScan, which builds on our observation of the interaction between 3D beams and 60 GHz SCPs. OScan can locate the optimal beam efficiently while reducing search latency by more than one order of magnitude (Sec. III).

(iii) We experiment with OScan using a custom-built 60 GHz software-radio along with a trace-driven emulator, and demonstrate its multi-fold throughput gain over state-of-the-art solutions (Sec. IV).

II. UNDERSTANDING LINK DYNAMICS IN 3-D SPACE

A. Mobility Measurement Setup

Different from previous works where mobility trajectories are generated by models or collected from controlled experiments [15], we investigate real-world mobility of two representative emerging applications, i.e., VR and Miracast, that rely on ultra-high-speed 60 GHz radios.

Wireless virtual reality: VR is anticipated to dominate future wireless multimedia application. However, a critical pain point is that a HDMI cable is required for transmitting VR data at multi-Gbps bitrate from a rendering server to the VR headset. The cable is not only cumbersome but also a potential safety hazard of tripping down users. Both industry and research communities have envisioned wireless VR over 60 GHz links [5], [6]. However, 60 GHz links are known to be highly unstable under mobility, and it remains unclear whether they can deliver seamless experience in the challenging mobile VR scenarios.

To elucidate this issue, we reproduce a typical VR setup (Fig. 1), and let a user play a typical VR game called "Magic Sunglass" [16] using a Lenovo Phab 2 Pro [17] equipped with a peripheral headset in an office building (Fig. 2). During the game, the user constantly moves, jumps and crouches in 3D space, and looks up/down/around as in a real gaming scenario. Phab [17] has built-in Google Tango [14], which incorporates depth cameras, motion tracking and computational vision technologies to enable mobile devices to detect their relative movement and orientation changes, with a spatial resolution of cm-level [18]. We build a customized Tango application running in background to record VR motion (including 3D translation and rotation) at a time interval of 10ms.

Before proceeding to detailed analysis in Sec. II-B, we present a 5-second snapshot of VR motion trace in Fig. 3. Here the black line represents the moving trajectory in 3D space, and the red arrow is the orientation at each sampling point. For figure clarity, we sample the orientation in steps of 10 points, *i.e.*, one arrow for each $100ms$. At first glance, neither the moving trajectory nor orientation follows any regular pattern (*e.g.*, linear or circular). Instead, many sudden trajectory/orientation shifts manifest, due to abrupt turning-back/looking-around actions of the VR players.

Miracast: Miracast allows a mobile device to duplicate its screen content to an external display with large screen (*e.g.*., TV or computer display monitor) via a wireless link, so as to support video casting, presentation sharing or interactive

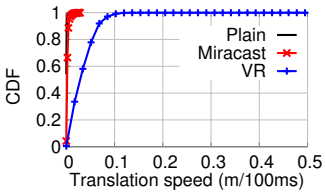

Fig. 4. CDF of translation speed.

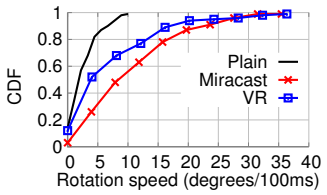

Fig. 5. CDF of YAW speed.

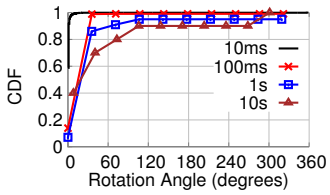

Fig. 6. YAW over different time scales.

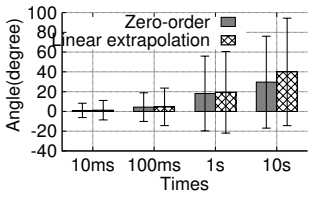

Fig. 7. VR Yaw prediction errors.

gaming in which the mobile device acts as a game controller and content generator. 60 GHz radios are widely considered as the enabling technology for high-definition Miracast, since it is hard to guarantee Miracast quality of experience (QoE) using the already-crowded 2.4GHz/5GHz WiFi. However, when delivering the video content to the display, the 60 GHz mobile Miracast device, held by the users, inevitably changes its position and orientation, which may jeopardize the application QoE. To investigate such practical effects, we reproduce the Miracast motion by hand-holding the Tango device, running a typical Miracast gaming application called "Doodle Jump" [19]. In what follows, we analyze the experimental results in detail.

B. 3D Mobility Analysis

Following the above setup, we have collected 3D movement traces from 10 users playing Miracast and VR, respectively. From the traces we compute translation (*i.e.*, movement along X, Y and Z axis in 3D space) and rotation (*i.e.*, roll, yaw, pitch) speeds at four different time intervals, $10ms$, $100ms$, $1s$ and $10s$. As a representative example, we plot the CDF of translation and rotation speeds in Fig. 4 and Fig. 5 at $100ms$ interval, *i.e.*, the default Beacon Interval (BI) of IEEE 802.11ad. For better understanding mobility characteristics of practical applications, we use plain mobility[1] as the baseline for comparison. We have the following major observations:

(i): In terms of translation, VR gaming [16] shows much more dynamic than Miracast gaming [19] and plain mobility. From Fig. 4, VR translation speed is up to 0.1 m/100ms (with mean of 0.03m/100ms) since VR players keep moving constantly. In contrast, translation speeds of Miracast and Plain are limited to 0.02m/100ms since users typically stand/sit statically during usage.

(ii): In terms of rotation, Miracast and VR show much more dynamics than plain mobility, since players keep rotating devices to catch interactive application scenes (Tab. I). In particular, rotation speed of Miracast is 3.9×, and that of VR is 2.7× over plain mobility, because hand rotation involved in Miracast (though the user may sit statically) is faster than head rotation in VR. Among Roll, Pitch and Yaw, Yaw rotation is the most dynamic. Such highest dynamic of Yaw roots from people's motion characteristic: VR players wearing the headset frequently look around or look up and down, but rarely swing left and right, and Miracast gaming users holding the devices wave their hand along Z-axis much frequently (Fig.1).

(iii) The Miracast/VR mobility shows strong dynamics at very short time scales. For instance, VR Yaw angle is usually larger than dozens of degrees even at a short time interval of 100 ms (Fig. 6). According to the 802.11ad standard [1], a full beam scanning process can take multiple or even dozens of Beacon Intervals (BIs), each lasting 100ms. Therefore, the scanning result may already become stale due to high rotation speeds. The observation clearly calls for an efficient beam steering mechanism in 3D space.

Unpredictability of mobility pattern: The high dynamics of 3D interactive applications imply that the motion patterns would be hardly predictable by using history records. We now quantitatively verify this conjecture. We use v_n to denote device orientation at time t_n, and then try to predict v_{n+1} given all v_i for $i \leq n$. We use two prediction methods: *(i): Zero-order prediction*, in which $v_{n+1} = v_n$ and *(ii): Linear extrapolation*, in which $v_{n+1} = v_n + (v_n - v_{n-1})(t_{n+1} - t_n)/(t_n - t_{n-1})$. As an example, we plot prediction errors of VR Yaw (*i.e.*, the gap between prediction and ground-truth) in Fig. 7, from which we have the following insights:

(i): The prediction errors are quite large, in terms of all rotation perspectives and time scales. For instance, the mean error of zero-order prediction is about 5° at 100ms intervals, which is way larger than 0.2° for plain mobility [20]. Moreover, the variance of prediction error is even lager (up to 20°), which again demonstrates high dynamic and randomness of 3D motion.

(ii): More importantly, prediction errors do not become smaller with increasing history information. In contrast, linear extrapolation with more history information sometimes performs even worse than zero-order prediction (Fig. 7). We have also tried more complicated prediction methods including high-order polynomial and exponential fitting, but cannot achieve more accurate prediction. We believe that the unpredictability lies in the inherent random nature of Miracast/VR motions. For instance, during VR games, the gaming scenarios constantly change due to multiple factors such as story evolution, interaction between user and the game, or interaction among users themselves. In order to match game scenarios, the user's location/posture/facing-direction will constantly change in an unrepeatable way.

The unpredictability also implies failure of heuristic based beam-steering methods. In particular, previous studies [8], [11] prioritize wider or neighbor beams after detecting device mobility, under the assumption that the next position will not be far from the previous one. While such shortcut may be useful under plain mobility, it becomes ineffective because the assumption is broken under 3D motion of interactive Miracast/VR. Experimental results in Sec. IV will further validate this point.

[1]Plain mobility represents movements during daily voice or data usage such as phone calls, Internet browsing and video watching, which is the default mobility model used in previous studies [20].

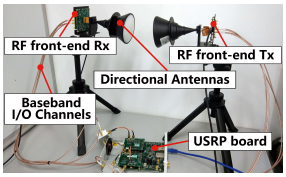

Fig. 8. 60 GHz radio platform.

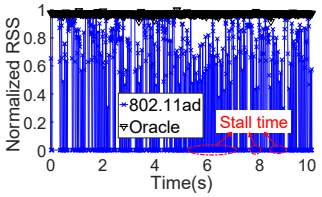

Fig. 9. A show case of link dynamic

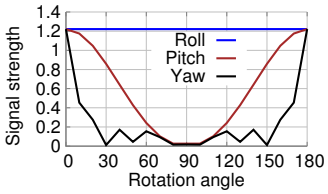

Fig. 10. Link quality vs. rotation.

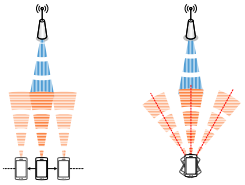

Fig. 11. Translation vs. rotation illu.

C. Link Dynamics

The channel quality of a 60 GHz link is determined by the interaction between two components: directional beamforming and the spatial channel profile (SCP). As shown in many previous studies, the SCP of 60 GHz radios is sparse, *i.e.*, signal arrives at any Rx only through a small number of paths, due to the pseudo-optical propagation property of 60 GHz signals [4], [8]. Channel quality will be the best when beamforming direction perfectly matches the SCP path with the strongest signal. Whenever there is a translation or rotation of transceivers, the beam direction and the strongest SCP path will become misaligned, which results in link quality degradation.

We examine link dynamics using a trace-driven emulation approach. In a nutshell, we first use a custom-built 60 GHz software-radio platform (a pair of Tx and Rx shown in Fig. 8) to collect SCPs of Rx at different location and orientation. Then we develop a MATLAB simulator to generate 3D directional beams using a 16×16 planar phased array, following a typical 802.11ad codebook [1]. Finally, we derive channel quality by convolving the SCPs and beams in the simulator[2]. In the following, we first showcase link dynamics along with a snapshot of practical VR movement, and then investigate the major factor behind link dynamics, *i.e.*, 3D rotation.

1) A showcase of link dynamics: In Fig. 9, we plot an RSS time-series over a 10-second mobility trace while a user is playing VR. We compare the performance of IEEE 802.11ad against an Oracle method. The 802.11ad method starts an hierarchical beam scanning once link quality drops below the lowest bit-rate threshold, whereas the Oracle can find the optimal beam with zero overhead. Overall, the mean RSS under 802.11ad is only 28.48% of that under Oracle. Such low performance roots in two facts: *(i)*: Due to ultra-high mobility dynamics, link quality can easily drop below the 802.11ad's lowest bitrate. In consequence, beam scanning is invoked very frequently, which leads to frequent and long *stall time*. *(ii)*: Even right after a channel scanning, the channel quality of 802.11ad is still much weaker than Oracle. The reason is that the optimal beam from scanning has already become stale as the device position/orientation has changed after the long stall time.

2) Impact of rotation: We keep the positions of Tx and Rx fixed, *i.e.*, 5 meters away along the X axis, and align their beam directions initially. Then we rotate Rx towards all 3D directions, *i.e.*, Roll, Pitch and Yaw over the range of [0, 180], and measure the result RSS during rotation (Fig. 10). A key observation is that a minor orientation change can result in abrupt drop of RSS. For instance, The RSS drop is more than 50% for less than 10° Yaw, which usually occurs in a very short time interval, 200∼300 ms, from measurements in Sec. II-B. Note that in this experiment Roll does not have impact on channel quality, because we set Tx/Rx facing each other along the X axis for simplicity.

[2]Such emulation approach is employed in most 60 GHz millimeter works, since there exists no programmable phased-array that allows low-level access to control directional beams. The accuracy and effectiveness of the approach have been extensively verified in previous studies [8], [13]

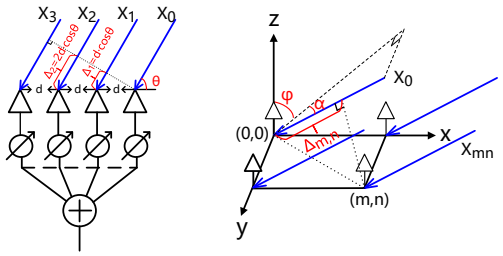

Fig. 12. Beam-forming on linear (left) and planar (right) phased array

Why rotation has such great impact? The reason lies in that the Tx/Rx beam mismatch caused by rotation is much more severe than that caused by translation. As illustrated in Fig. 11, suppose the initial Tx/Rx distance is d meters, then a x meters translation will result in a beam mismatch of $\arctan(\frac{x}{d})$. For instance, the mismatch angle is only about 9° when $d = 10$ and $x = 1$ (*i.e.*, the user moves 1 meter, which may take tens of seconds in practical VR/Miracast usage). Moreover, the mismatch decreases with d. In contrast, a slight hand or head rotation (which happens in a few milli-seconds in Miracast or VR) may cause orientation difference of dozens of degrees, which leads to severe Tx/Rx beam mismatch, irrespective of the value of d. As a result, rotation has much more severe impact on link dynamics.

III. OScan Design

In this section, we first model the unique interaction between 3D beams and 60 GHz SCPs, and then present how OScan's model-driven beam steering works by exploiting the interaction.

A. Modeling Interaction between 3D Beams and SCPs

As noted before, the channel quality of a 60 GHz link is determined by the interaction between beam-forming gain and the underlying SCP. In Fig. 13, we plot a typical 3D beam generated by a 16×16 phased array, and the main-lobe direction is set to $\{30^\circ, 30^\circ\}$, *i.e.*, both azimuth angle ψ and elevation angle α are 30°. Intuitively, the 3D beam looks like a "deformed cross", where the main-lobe lies in the intersection of the cross, and the side-lobes distribute along two wing-like sides. Such "deformed cross" remains consistent irrespective of array size and beam direction, as we will model later.

From a Rx's perspective, the ideal case is that the main-lobe of its current beam overlaps perfectly with the strongest

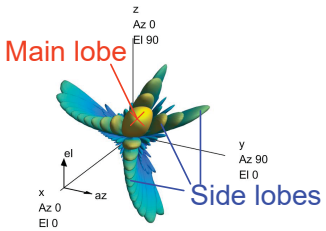

Fig. 13. An example 3D beam

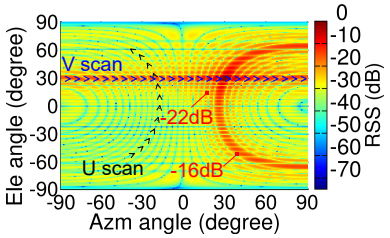

Fig. 14. Beam RSS distr. and OScan procedure

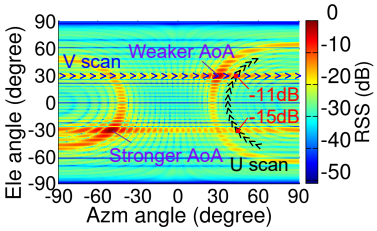

Fig. 15. Multi-AoA issue

Angle of Arrival (AoA) of the SCP, which will lead to the strongest channel quality. In addition, a beam whose side-lobe overlaps with the AoA may also bring satisfactory sub-optimal channel quality. More importantly, we find that the side-lobes has profound effects in 3D case, which is different from the 2D case. In particular, a conventional wisdom is that a closer beam (*i.e.*, its main-lobe direction is close to the AoA in terms of angular separation) achieves better channel quality than further-away beams. However, we find that the case can be totally opposite under 3D scenarios. For instance, we plot the channel quality of all 3D beams, given an AoA of $\{30°, 30°\}$ in Fig. 14. As marked in the figure, the further-away beam with main-lobe direction of $\{40°, -50°\}$ has 6dB higher RSS than the much closer beam with direction of $\{20°, 15°\}$.

UV mapping: To generalize and model the above findings, we examine it from another perspective. For any 3D direction represented by $\{\psi, \alpha\}$ (ψ is the azimuthal angle, and α is the elevation angle, $\psi, \alpha \in [-90, 90]$), we can map it to a point $\{u, v\}$ in UV space[3] as follows,

$$\begin{aligned} u &= \cos(\alpha)\sin(\psi) \\ v &= \sin(\alpha) \end{aligned} \tag{1}$$

Using this UV coordinate system, we re-plot Fig.14, and the result is given in Fig. 16. From the figure, we observe a clear "cross" feature: the beams with non-negligible RSS distribute along two orthogonal lines: $\{u^*, :\}$ and $\{:, v^*\}$ with intersection point $\{u^*, v^*\}$, which is the UV coordinate corresponding to the AoA direction, *i.e.*, $\{30°, 30°\}$).

Modeling the interaction: in a nutshell, the "cross" feature is formed by the joint effect of 60 GHz signal propagation and beamforming effect of phased array.

Signal propagation effect: The far-field model is usually adopted to model 60 GHz signal propagation, due to very short wavelength of 60 GHz radio [8], [22]. As illustrated in Fig. 12, incoming signals arrive at a 4-element linear phased-array (with element space of d) in parallel from direction θ, and signal at m_{th} element is denoted with x_m ($m \in [0, 3]$). Then we can calculate the difference of propagation path length between signal x_m and x_0, denoted with Δ_m as follows,

$$\Delta_m = md\cos(\theta) \tag{2}$$

Translating the path length difference to phase difference δ_m between signals of element 0 and element m, we have

$$\delta_m = 2\pi\Delta_m/\lambda \tag{3}$$

where λ is the wavelength. As a result, we have the relation between signal x_m and x_0 as follows,

$$x_m = x_0 \exp^{j\delta_m} \tag{4}$$

[3]UV mapping is a classical 3D modeling process that maps a 3D surface to a 2D texture [21], which is widely used in 3D graphics domain.

Here we focus on phase change but omit minor signal amplitude change which is negligible due to very short distance among phased array elements [22].

We then extend the above model to a 2D planar phased-array, which can generate 3D beams in practice. As shown in Fig. 12, we assume a $M \times N$ phased array, and incoming signals from azimuth angle ψ and elevation angle α. Similarly, the phase difference between antenna A_{mn} and A_{00} can be computed as follows,

$$\delta_{mn} = \exp^{j2\pi(nd\cos(\alpha)\sin(\psi)+md\sin(\alpha))/\lambda} \tag{5}$$

and the signal arriving at A_{mn} is as follows,

$$x_{mn} = x_{00}\delta_{mn} \tag{6}$$

where x_{00} is the signal at A_{00}.

Beamforming effect: We denote the beamforming weight on A_{mn} with w_{mn} (under power constraint of $\sum_{\forall m,n} \|w_{mn}\|^2 = 1$), the overall signal after beamforming is,

$$r = \sum_{m=0}^{M}\sum_{n=0}^{N} w_{mn}x_{mn} = x_{00}\sum_{m=0}^{M}\sum_{n=0}^{N} w_{mn}\delta_{mn} \tag{7}$$

From Eq. (7), if we want to maximize the signal from direction $\{\psi, \alpha\}$ (*i.e.*, beam-forming to the direction), the beamforming weight w_{mn} should be the reciprocal of phase change δ_{mn},

$$w_{mn} = \frac{1}{\delta_{mn}} = \exp^{-j2\pi(nd\cos(\alpha)\sin(\psi)+md\sin(\alpha))/\lambda} \tag{8}$$

Generally, given any beam pointing to direction $\{\psi, \alpha\}$, *i.e.*, its beamforming weight is Eq. (8), the channel response for an incoming signal from a fixed AoA direction of $\{\psi^*, \alpha^*\}$ is,

$$r_{\psi\alpha} = x_{00}\sum_{m=0}^{M}\sum_{n=0}^{N} \exp^{j2\pi nd(u^*-u)/\lambda}\exp^{j2\pi md(v^*-v)/\lambda} \tag{9}$$

where $u^* - u = \cos(\alpha^*)\sin(\psi^*) - \cos(\alpha)\sin(\psi)$ and $v^* - v = \sin(\alpha^*) - \sin(\alpha)$. From Eq. (9), for an arbitrary u, the channel will be stronger when $v = v^*$. Similarly, for an arbitrary v, the channel will be stronger when $u = u^*$. In consequence, the line $\{\forall u, v^*\}$ with stronger channel forms the horizontal line in Fig. 16, and $\{u^*, \forall v\}$ forms the vertical line.

B. Model-driven Beam Scanning

Inspired by the "cross" feature, we design OScan such that it can find the optimal beam direction, *i.e.*, the intersection point $\{u^*, v^*\}$ in Fig. 16 with minimal scanning overhead. The basic process includes two simple but effective steps. First, OScan scans vertically along an arbitrary U layer, *i.e.*, it tries all beams of $\{u_0, v\}$, where u_0 is randomly selected and $v \in [-1, 1]$. The scanning line (formed by the scanning beams) will intersect the horizontal stripe of the "cross" at a point denoted with

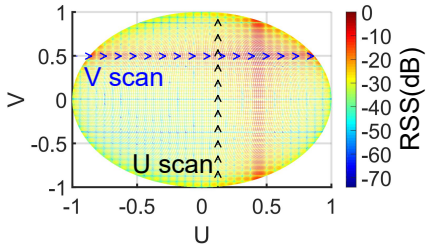

Fig. 16. Beam response after UV mapping

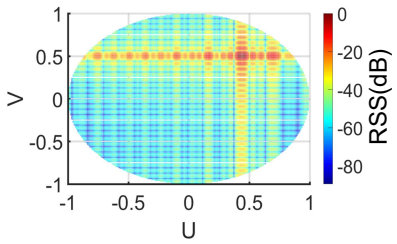

Fig. 17. Beam response w/ discrete codebook

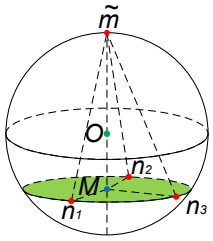

Fig. 18. Finding the $4th$ start beam

$\{u_0, v^*\}$, which has the maximum channel quality among all scanning beams. Second, OScan scans horizontally along the V layer of v^*, and then it finds the intersection of $\{u^*, v^*\}$. Note that the scanning sequence can also be opposite, *i.e.*, scanning along V layer and then along U layer. Mapping the process back to the azimuthal-elevation dimension, OScan works in practice as follows, including two steps as shown in Fig. 14:

(i) U scan: OScan scans all beams that satisfy $\cos(\alpha)\sin(\psi) = u_0$, where u_0 is arbitrarily selected. In particular, the range of scanning elevation angle is $[\arcsin(-\sqrt{1-u_0^2}), \arcsin\sqrt{1-u_0^2}]$ from Eq. (1). Let ω be the scanning angle resolution, then there are $W_1 = 2\arcsin(\sqrt{1-u_0^2})/\omega$ beams to be scanned. For i_{th} beam ($i \in [1, W_1]$), we have

$$\begin{aligned} \alpha_i &= \arcsin(-\sqrt{(1-u_0^2)} + (i-1)\omega) \\ \psi_i &= \arcsin(u_0/\cos(\alpha_i)) \end{aligned} \tag{10}$$

We denote the optimal beam with maximum channel quality using $\{\psi^{'}, \hat{\alpha}\}$ after U scan.

(ii) V scan: Then we scan with fixed elevation angle $\hat{\alpha}$ and all possible azimuthal angles. Specifically,

$$\begin{aligned} \alpha_i &= \hat{\alpha} \\ \psi_i &= -\pi/2 + (i-1)\omega \end{aligned} \tag{11}$$

where $i \in [1, W_2]$ and $W_2 = \pi/\omega$. The optimal beam after the scanning, $\{\hat{\psi}, \hat{\alpha}\}$, *i.e.*, the beam with the maximum channel quality, is deemed as the estimation of the ground-truth AoA direction $\{\psi^*, \alpha^*\}$.

1) Handling multiple AoAs: So far we focus on the basic case that only one AoA exists. In practice, signals may arrive in clusters along multiple AoAs (from the LoS path or NLoS paths), and OScan may stop at a local maximum point (*i.e.*, an AoA with smaller RSS) instead of the global optimum, if the initial scanning direction is close to weaker AoAs. We demonstrate the problem in Fig. 15, in which we set two AoAs, and intentionally make the starting beam of OScan closer to the weaker AoA (the upper right one). During U scan, OScan encounters the two "deformed cross" formed by the two AoAs, successively. Unfortunately, the second encounter point with the weaker AoA has a larger RSS of -11dB, which finally leads the consequent V scan to the weaker AoA.

To solve this problem, OScan runs multiple rounds (say, K rounds) of U&V scan, each round with a new starting beam direction. In particular, we strategically set the new starting beam $\tilde{m}$ to be furthest from beams outputted from previous rounds, in order to get the most complementary scanning. We determine $\tilde{m}$ as follows. First, we define $\eta_{m,n}$, the distance between two beams as the l_1 norm of the difference between their main-lobe directions $b(m)$ and $b(n)$, respectively,

$$\eta_{m,n} = \|b(m) - b(n)\|_1 \tag{12}$$

Based on this pairwise distance, we further define the distance between a beam m and the *set of beams found in previous rounds*, Ω, as follows,

$$\zeta_{m,\Omega} = \min_{n \in \Omega} \eta_{m,n} \tag{13}$$

Then, the next starting beam $\tilde{m}$ is determined as the one with the largest distance to Ω,

$$\tilde{m} = \arg \max_{m \in all\_beams} \zeta_{m,\Omega} \tag{14}$$

In practice, we can use geometrical knowledge to determine $\tilde{m}$, without incurring extensive computation of Eq. (14), when Ω is small. For instance, in Fig. 18, when $|\Omega| = 3$ (*i.e.*, $\Omega = \{n_1, n_2, n_3\}$), the 4_{th} starting beam direction $\tilde{m}$ is the intersection point of the sphere and the line MO, which is the connection line of the sphere center O and the circumcenter M of the surface defined by n_1, n_2 and n_3. The pseudo-code Alg. 1 summarizes the operations of OScan.

Algorithm 1 OScan

INPUT: The set of all beams Ω, # of loops K
OUTPUT: Steering direction $\{\hat{\psi}, \hat{\alpha}\}$
Set of potential optimal beams Ω = [ ]
k = 0;
$u_0 \leftarrow$ an arbitrary beam direction;
/* Iterative loop*/
while $k < K$
    /*Scanning along V dimension with fixed u_0*/
    Scan with $\forall\{\psi_i, \alpha_i\}$ from Eq. (10)
    $\{\psi^{'}, \hat{\alpha}\} \leftarrow$ the beam with the strongest channel
    /*Scanning along U dimension with fixed $v = \sin(\hat{\alpha})$*/
    Scan with $\forall\{\psi_i, \alpha_i\}$ from Eq. (11)
    $\{\hat{\psi}, \hat{\alpha}\} \leftarrow$ the beam with the strongest channel
    Ω = $\Omega \cup \{\hat{\psi}, \hat{\alpha}\}$
    /*Deciding the start direction for next loop*/
    $\tilde{m} \leftarrow$ the beam computed from Eq. (14)
    $u_0 \leftarrow$ UV mapping result of $\tilde{m}$ from Eq. (1)
    $k = k + 1$
endforwhile
$\{\hat{\psi}, \hat{\alpha}\} \leftarrow$ the best beam in Ω with maximum RSS

2) Code-book independence of OScan: From above, we can observe that OScan's gain is not tied to any particular codebook, but stems from the essential interaction between analog beamforming and signal propagation effect over the planar phased array. Specifically, beam weights in Eq. (8) reflects the general

codebook design principle that is widely adopted in CTOS phased array [22] and 802.11ad standard [1].

Despite the common principle, one concern is that 60 GHz analog phased array cannot choose arbitrary phase shift as weight (Eq. (8)), since each antenna element is controlled by a phase shifter that supports a discrete set of phases denoted with Γ, *e.g.*, $\Gamma = \{0, \pi/2, \pi, 3\pi/2\}$ for a 2-bit phase shifter. However, we find that it does not have substantial impact on beam patterns or steering performance. The reason is that a beamforming direction is a compound effect of all elements, which together goes beyond the limited set of discrete phases and can support a huge set of beam directions. In particular, a Q-element phased array (each element supports P phases) can point to P^Q directions [23]. We plot the channel quality over all beams of a 32×32 phased array with 2-bit shifter in Fig. 17 after taking into account the discretization effect, *i.e.*, we map ideal phases used in Eq. (8) to the closest discrete one in Γ according to standards [1], [23]. Clearly, the "cross" property is well preserved as in Fig. 16 except an overall channel quality degradation caused by the discretization. Moreover, we use the 802.11ad discrete codebook [1] in our evaluation (Sec. IV), where the multi-fold gain further validates the efficacy of OScan after taking into account the discretization effect.

In addition, hierarchical code-books are adopted in 802.11ad [1] to accelerate beam steering. In particular, 802.11ad first scans with quasi-omni beams, which narrows beam searching space into a sector range. Then fine-grained beam scanning is performed inside the narrow sector to locate the optimal beam with less overhead. Similarly, OScan can naturally integrate with such a hierarchical principle by setting multiple levels of hierarchy when doing the "cross" searching. Due to space limit, we omit the details. We emphasize that OScan still outperforms 802.11ad significantly since it saves scanning overhead in each level of hierarchy, as demonstrated in Sec. IV.

3) Overhead analysis: OScan scans K rounds, each round with $M + N$ beams (here M and N is the number of beams along azimuth and elevation dimension, respectively), and in total OScan uses $K(M + N)$ beams. It is worth noting that K is typically less than 5 in practice (as will be validated in Sec. IV-B) due to spatial sparsity of the 60 GHz channel [8], [24]). Suppose M and N are of the same order, then the scanning overhead of OScan will be $O(N)$, which is linear, in contrast to the quadratic complexity of 802.11ad [1], [8]. When we consider beam scanning on both Tx and Rx, the overall overhead will be the multiplication of overhead on both sides, *i.e.*, $O(N^2)$ for OScan and formidable $O(N^4)$ for 802.11ad.

IV. Evaluation

A. Implementation and Evaluation Methodology

We adopt a trace-driven emulation approach for evaluation. *First*, we have custom-built a 60 GHz software radio platform, which operates on 57-64 GHz and do channel measurements using mechanically rotated horn antennas (Fig. 8). Meanwhile, we use Google Tango to record 3D motion during VR/Miracast usage. *Second*, we develop a mmWave simulator that can generate 3D beams with various phased-arrays, using 802.11ad codebooks. Feeding with collected channel and mobility traces, the simulator can emulate and evaluate beam-steering effect over practical mobile applications. It is noteworthy that such trace-driven emulation approach has been verified and commonly employed in previous studies [4], [12], [13], [24].

For comparison, we have also implemented the default beam-scanning of IEEE 802.11ad, and heuristic approach (Heu) widely used in state-of-the-art [8], [25], which opportunistically exploits wider beams and sub-optimal backup beams from last-round scanning. In the following, we first examine OScan's convergence speed, accuracy and overhead in mirco-benchmark evaluation, and then we evaluate its system-level performance under different application and environment configurations.

B. Micro-benchmark Evaluation

1) Convergence: As shown in Alg. 1, OScan uses K rounds of scanning in order to avoid local optimum. Clearly, K is a key parameter for final link performance: a larger K leads to stronger AoA and better channel quality, but also indicates more scanning overhead. We investigate such a trade-off by examining channel quality under different K values. In particular, we select a segment consisting of 100 random consecutive points from a VR motion trace. We run OScan over the segment using a 16x16 phased array, while increasing K from 1 to 10. We repeat the experiments using different SCP configurations, *i.e.*, SCPs consisting of 1, 3, 5, 7 signal paths (*i.e.*, AoAs) respectively. From the results in Fig. 19, we can observe that OScan converges very quickly, irrespective of number of AoAs. In particular, link RSS with $K = 4$ is above 95% of that under $K = 10$, and is 12dB higher than that under $K = 1$ on average. In later experiments, we set $K = 4$, and we will find that it achieves remarkable performance under various scenarios. A rigorous analysis of OScan's convergence is an interesting problem but out of the scope of this paper.

2) Accuracy: Now we compare the RSS of OScan's converged beam against that of the optimal beam derived from "Oracle". We experiment with different phased-array sizes and fixed $K = 4$, while keeping other configurations the same with the above experiment. From the results in Fig. 20, we have two observations: *(i)* RSS of OScan is very close to the optimum, irrespective of phased-array size. In particular, the mean RSS ratio of OScan over Oracle is about 95.2% over all arrays, which clearly validates the high accuracy of OScan's model-driven scanning. *(ii)* The ratio decreases a little bit for the largest 32x32 phased array, because the beams become quite narrow and it is harder for OScan to locate exactly the perfect beam. Despite this, OScan still achieves as high as 89.3% RSS of the Oracle.

3) Overhead: In Sec. III, we have analyzed that the overhead (*i.e.*, number of all scanning beams) of OScan is on a liner order, while that of 802.11ad scanning is of quadratic order, when considering beam steering on one of Tx or Rx side. Now we compare the actual time spent on beam steering, according to IEEE 802.11ad time specification (*i.e.*, $7\mu s$ for each beam [1], [8]) in Fig. 21, and make the following observations: *(i)* As expected, OScan has remarkably low scanning overhead. Moreover, its advantage becomes increasingly profound on larger phased-arrays. In particular, the beam-steering latency of 11ad beam searching increases rapidly from $0.3ms$ to $47ms$ for a 32x32 phased array. It is an overwhelming overhead since about half of channel time will be spent on beam steering (considering the fact that beam steering can be evoked in

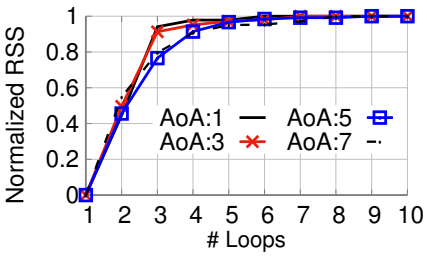

Fig. 19. OScan's convergence.

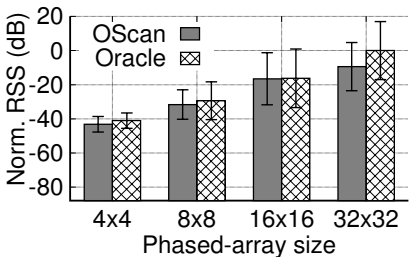

Fig. 20. Channel quality comparison.

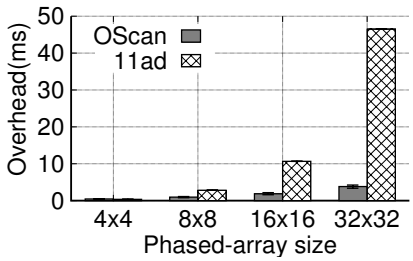

Fig. 21. Scanning overhead comparison.

intervals of less than $100ms$ according to Sec. II). On the other hand, OScan bounds the steering latency below $4ms$. *(ii)* The overhead of 11ad scanning can become formidable ($2.5s$ vs. $15ms$ of OScan) when considering simultaneous scanning on both Tx and Rx, which will happen when both Tx/Rx are mobile or the translation speed on one side is very fast.

To sum up, OScan achieves above 95% RSS of the optimum with less than 20% overhead on average.

C. System-level Evaluation

1) Throughput gain over different applications: We record the mobility trace while a user is playing VR [16] and Miracast [19] game, respectively, and then feed the trace into our simulator to get link throughput, after integrating beamforming gain, beam steering overhead and 802.11ad timing operations into a system-level framework [4] From the results in Fig. 22, we have the following observations: *(i)* OScan significantly outperforms the two methods. Specifically, the average throughput gains over 802.11ad are about 1.9× and 5.6× under VR and Miracast scenarios, respectively. The results corroborate the mobility measurement in Sec. II, where Miracast is more dynamic than VR in term of rotation movement. Therefore, Miracast movement has a more severe effect on link performance, and leaves larger space for improvement. *(ii)* Compared with the baseline 802.11ad, Heu shows quite marginal gain or even worse performance, which is the opposite of the 2D case [11]. Again, the reason lies in that wider or nearby beams used in Heu are no longer effective backups, due to the high dynamics of 3D movement.

2) Throughput gain over different reflecting environments: We examine VR performance of OScan under increasingly-complicated environments. In particular, the environment is mapped from a typical office (Fig. 2) into our ray-tracing emulator. We then add planar reflectors into the emulated environment and increase the number of reflectors from 1 to 6. The LoS path is blocked for the first two environments. From the results in Fig. 23, we have two observations: *(i)* The LoS path plays a substantial role in network performance. For environment 1 and 2, the throughput is still very low even OScan achieves about 1.5× gain, due to absence of strong LoS path. *(ii)* Heu becomes less efficient compared with 802.11ad as the environment becomes more complicated, because wider backup beams in Heu have a larger probability to align with one sub-optimal AoA due to the existence of multiple reflectors, which keeps Heu running at a low bit-rate.

[4]Here the we focus on performance index of throughput. We plan to extend the simulation to packet level, so as to investigate delay and jitter indices, which are also very important to real-time applications.

3) Throughput gain over different users: To study the effect of individual mobility, we recruit 10 volunteers to play the same VR game [16] and measure each one's throughput during usage. From Fig. 24, we can observe different impact of mobility on link performance, arising from the different reactions of individuals to the VR gaming scenarios. For instance, user 7's engagement to the VR game is less and thus her movement is slower, which leads to higher performance under 802.11ad and Heu. However, despite individual variation, the gain of OScan remains consistent, *i.e.*, 1.7× and 1.8× on average over 802.11ad and Heu, respectively.

V. Related Works

Amid the exacerbation of wireless bandwidth crisis [26] and maturity of protocol standardization [1], mmWave, particularly the unlicensed 60 GHz radios, has been attracting more and more attention. Recently, much research effort has been devoted to experimental and system-level 60 GHz radio research [3]–[6], [8], [11]–[13], [27], [28], based on prior theoretical works (see [29] and references therein). 60 GHz radios are widely considered as the enabling technology for the emerging wireless VR [5] or 4K/8K Miracast [7] with multi-Gbps bitrate requirement. In particular, recent works in [6], [30] designed 60 GHz relay or multiple-AP architecture to boost wireless VR performance.

Beam steering is one of the most critical factors on 60 GHz system-level performance. Extensive research has verified the inefficiency of the default beam steering in legacy standards and proposed solutions [11]–[13], [24], [27]. In particular, BBS [27] couples 60 GHz radio with an extra 2.4/5 GHz WiFi module, and leverages inference from the lower-frequency channel to speed up beam steering. Beamspy [24] develops a prediction model to estimate beam quality and switch to the alternative beam under blockage. E-Mi [12] and Beamforecast [13] exploit the high-resolution sensing ability of 60 GHz radios to reconstruct ambient environment, and leverage the environment information (such as reflectors' location and reflectivity) to optimize AP deployment and mobile user tracking, respectively. However, these systems all focus on 2D beam steering, and neglect the unique characteristics of 3D movement and their impact on link performance.

Besides theoretical works [35], [36], 3D beamforming of 60 GHz radios and its application in wireless data centers (DC) has been studied in [31]–[33]. Our work differs in two major aspects: *(i)* These works focus on *static* scenarios where 60 GHz radios are mounted on DC racks or containers. *(ii)* These works only consider perfect directional beams created by mechanically-rotated horn antennas, but neglect the codebook

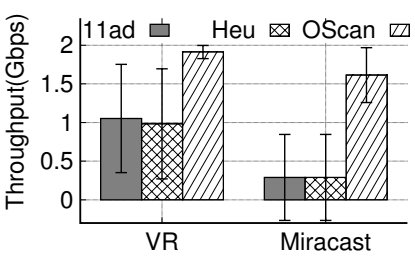

Fig. 22. Throughput vs. application.

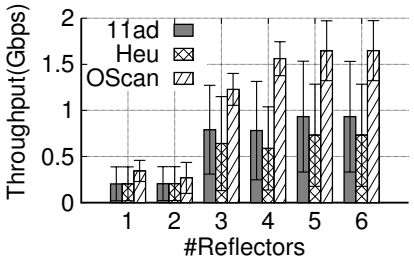

Fig. 23. Throughput vs. environment

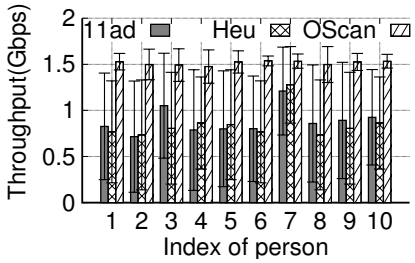

Fig. 24. Throughput vs. person.

based phased-array beamforming. In contrast, we model the interaction between codebook based beamforming and spatial channel profile, and design a model-driven 3D beam-steering by exploiting the un-known interaction. In addition, there are also works devoted to 3D beamforming at lower-frequencies (Wi-Fi or LTE frequencies, see [20], [34] and references therein), but they are much different from our work due to fundamentally different channel characteristics.

VI. Conclusion

In this paper, we have measured and analyzed 3D movement characteristics of practical wireless VR and Miracast applications, and demonstrated their severe adverse effect on directional 60 GHz wireless communication. On the other hand, we find that there exists a unique interaction between 3D beams and spatial channel profile of 60 GHz radios. Based on the observations, we propose a model-driven 3D beam-steering mechanism called OScan, which converges to the optimal beam with minimal beam scanning overhead, and thus brings multi-fold throughput gain under various practical settings. In future, we plan to investigate the usage of OScan in multi-cell 60 GHz networks, in which we will consider the integration of OScan with other 60 GHz networking primitives, such as multi-AP handoff and interference management.

VII. Acknowledgment

The work reported was supported in part by the National Natural Science Foundation of China (No.61772084, No.61720106007, No. 61332005 and No. 61532012). Teng Wei and Xinyu Zhang were supported in part by US NSF funding CNS-1350039, CNS-1506657, CNS-1518728 and CNS-1617321.

References

[1] IEEE Standards Association, "IEEE Standards 802.11ad-2012: Enhancements for Very High Throughput in the 60 GHz Band," 2012.
[2] "IEEE 802.11ay," http://www.ieee802.org/11/Reports/tgay_update.htm, Jul. 2017.
[3] T. Rappaport *et al.*, "Millimeter Wave Mobile Communications for 5G Cellular: It Will Work!" *IEEE Access*, vol. 1, 2013.
[4] Y. Zhu *et al.*, "Demystifying 60ghz outdoor picocells," in *ACM MobiCom*, 2014.
[5] "Desperately seeking wireless: VR's aiming to cut the cord," https://www.cnet.com/news/vr-desperately-seeking-wireless/, 2017.
[6] O. Abari, D. Bharadia, A. Duffield, and D. Katabi, "Enabling high-quality untethered virtual reality," in *USENIX NSDI*, 2017.
[7] W.-F. Alliance, "Wi-fi display technical specification v1.2n," 2011.
[8] S. Sur *et al.*, "60 ghz indoor networking through flexible beams: A link-level profiling," in *ACM SIGMETRICS*, 2015.
[9] IEEE Standards Association, "IEEE Standards 802.15.3c-2009: Millimeter-wave-based Alternate Physical Layer Extension," 2009.
[10] N. T, A. B. Flores, E. W. Knightly, and J. Widmer, "Steering with eyes closed: mm-wave beam steering without in-band measurement," in *IEEE INFOCOM*, 2015.
[11] M. K. Haider and E. W. Knightly, "Mobility resilience and overhead constrained adaptation in directional 60 ghz wlans: Protocol design and system implementation," in *ACM MobiHoc*, 2016.
[12] T. Wei, A. Zhou, and X. Zhang, "Facilitating robust 60 ghz network deployment by sensing ambient reflectors," in *USENIX NSDI*, 2017.
[13] A. Zhou, X. Zhang, and H-D Ma, "Beam-forecast: Facilitating mobile 60 ghz networks via model-driven beam steering," in *IEEE INFOCOM*, 2017.
[14] "Tango(platform)," https://en.wikipedia.org/wiki/Tango_(platform), 2017.
[15] T. Camp, J. Boleng, and V. Davies, "A survey of mobility models for ad hoc network research," *Wireless Communications and Mobile Computing*, vol. 2, no. 5, 2002.
[16] "Magic Sunglasses," http://www.utovr.com/video/251711033593.html, Jul. 2017.
[17] "Lenovo phab 2 pro," https://en.wikipedia.org/wiki/Lenovo_Phab_2_Pro, 2017.
[18] R. Roberto, J. P. Lima, T. Arajo, and V. Teichrieb, "Evaluation of motion tracking and depth sensing accuracy of the tango tablet," in *IEEE ISMAR-Adjunct*, Sept 2016, pp. 231–234.
[19] "Doodle Jump," http://doodlejumponline.org, Jul. 2017.
[20] A. Amiri Sani, L. Zhong, and A. Sabharwal, "Directional antenna diversity for mobile devices: Characterizations and solutions," in *ACM MobiCom*, 2010.
[21] "Uv mapping," https://en.wikipedia.org/wiki/UV_mapping, 2017.
[22] D. Huang, R. Nandakumar, and S. Gollakota, "Feasibility and limits of wi-fi imaging," in *ACM SenSys*, 2014.
[23] M. E. Rasekh, Z. Marzi, Y. Zhu, U. Madhow, and H. Zheng, "Noncoherent mmwave path tracking," in *ACM HotMobile*, 2017.
[24] S. Sur, X. Zhang, P. Ramanathan, and R. Chandra, "Beamspy: Enabling robust 60 ghz links under blockage," in *USENIX NSDI*, 2016.
[25] M. K. Haider and E. W. Knightly, "Mobility resilience and overhead constrained adaptation in directional 60 ghz wlans: Protocol design and system implementation," in *ACM MobiHoc*, 2016.
[26] Qualcomm Inc., "The 1000x Data Challenge," https://www.qualcomm.com/1000x, 2014.
[27] N. T, A. B. Flores, E. W. Knightly, and J. Widmer, "Steering with Eyes Closed: mm-Wave Beam Steering without In-Band Measurement," in *IEEE INFOCOM*, 2015.
[28] T. Nitsche, G. Bielsa, I. Tejado, A. Loch, and J. Widmer, "Boon and bane of 60 ghz networks: Practical insights into beamforming, interference, and frame level operation," in *ACM CoNEXT*, 2015.
[29] H. Xu, V. Kukshya, and T. S. Rappaport, "Spatial and temporal characteristics of 60-ghz indoor channels," *IEEE JSAC*, vol. 20, no. 3, pp. 620–630, Apr 2002.
[30] T. Wei and Z. XinYu, "Pose information assisted 60 ghz networks: Towards seamless coverage and mobility support," in *ACM MobiCom*, 2017.
[31] W. Zhang, X. Zhou, L. Yang, Z. Zhang, B. Y. Zhao, and H. Zheng, "3d beamforming for wireless data centers," in *ACM HotNets*, 2011.
[32] X. Zhou, Z. Zhang, Y. Zhu, Y. Li, S. Kumar, A. Vahdat, B. Y. Zhao, and H. Zheng, "Mirror mirror on the ceiling: Flexible wireless links for data centers," *SIGCOMM CCR*, 2012.
[33] Y. Cui, S. Xiao, X. Wang *et al.*, "Diamond: Nesting the data center network with wireless rings in 3d space," in *USENIX NSDI*, 2016.
[34] H. Halbauer, S. Saur, J. Koppenborg, and C. Hoek, "3d beamforming: Performance improvement for cellular networks," *Bell Labs Technical Journal*, vol. 18, no. 2, pp. 37–56, Sept 2013.
[35] M. K. Samimi and T. S. Rappaport, "3-d statistical channel model for millimeter-wave outdoor mobile broadband communications," in *IEEE ICC*, 2015.
[36] W. Zou, L. Wang, and C. Guo, "3d-beamforming codebook design based on directly search for millimeter-wave communications," in *IEEE INFOCOM*, 2016.